Nondestructive corrosion detection using fiber optic photoacoustic ultrasound generator

Xiaotian Zou [a], Tyler Schmitt [b], David Perloff [c], Nan Wu [b], Tzu-Yang Yu [c], Xingwei Wang [a,b,*]

[a] Department of Biomedical Engineering and Biotechnology, University of Massachusetts, Lowell, MA 01854-2827, United States
[b] Department of Electrical and Computer Engineering, University of Massachusetts, Lowell, MA 01854-2827, United States
[c] Department of Civil and Environmental Engineering, University of Massachusetts, Lowell, MA 01854-2827, United States

ARTICLE INFO

ABSTRACT

Ultrasonic technologies have been widely used in nondestructive and noninvasive testing applications in industry. In this paper, a study on novel nondestructive corrosion detection mechanism with fiber optic photoacoustic ultrasound generator is conducted. The presented corrosion detection mechanism features compact device size (ideal for embedded optical fiber applications), non-contact approach, stable performance, and high spatial resolution. The principle of ultrasonic corrosion detection is introduced in the first section. The experimental procedure for simulation and acceleration of the sample corrosion by using the electrochemical process is also presented. Three steel reinforced rebar samples were prepared with different corrosion rates. The rebar samples were characterized to demonstrate that our mechanism is an effective tool in detecting the corrosion level of steel rebar samples.

Published by Elsevier Ltd.

1. Introduction

Rebar corrosion has proven to be the culprit in a significant portion of reinforced concrete structural failures [1]. Rebars, which form a supportive lattice in concrete, are meant to handle the tensile demands on the structures in which they are implemented. Without their additional strength, concrete structures become vulnerable to these tensile loads, and the chances of catastrophic failure increase dramatically [2].

The corrosion process has a drastic economic toll, the Federal Highway Administration has reported that the cost of rebar corrosion related repairs average about $286 billion per year [3]. In addition to monetary and infrastructure concerns, the resulting detriment to human security

must be addressed. Many structural failures, especially those of buildings and bridges, pose significant safety threats that cannot be ignored [4].

The corrosion process is typically attributed to the use of deicing salts in snow hazards and salt water corrosion near the shores. The surrounding concrete can protect rebars from corrosion with a high alkaline environment, but the inevitable formation of micro-cracks from strain provides multiple points of entry for corrosive materials. Chloride ions are notoriously aggressive corrosives of refined steel products, like rebars [4,5].

The best way to mitigate safety, economic, and infrastructure concerns is the early detection of this process and the swift repair of affected rebars. Tests and measurements must also be done nondestructively in order to be cost-effective. There are multiple nondestructive techniques that are used to estimate the extent of corrosion in practice today. Some methods, such as open circuit potential, surface potential, and concrete resistivity measurements, attempt to detect indications of the

* Corresponding author at: Department of Electrical and Computer Engineering, University of Massachusetts, Lowell, MA 01854-2827, United States.

E-mail address: Xingwei_Wang@uml.edu (X. Wang).

electrochemical reactions caused by the corrosion process [5–7]. These methods can be effective, yet are vulnerable to many other largely unpredictable electrochemical processes in the steel–concrete environment, and several require direct contact with the rebar [5].

Ultrasonic testing is one method that has impressive potential in detecting rebar corrosion where destructive testing is not desirable. Many detection methods based on ultrasonic pulse-transmission, pulse-echo, impact-echo and resonance techniques exist to quantify chemical damage in concrete [8–10]. However, the resolution of such detection techniques is limited by the bandwidth of the ultrasound generator. High resolution detection usually requires an ultrasonic generator featuring wide bandwidth. The wide bandwidth (5 MHz) ultrasonic electrostatic transducers have been applied to detect the internal corrosion in concrete structure [11]. The broadband ultrasonic transducer provides much better resolution of measurements. However, signal attenuation increases as the wave penetrates deeper inside the concrete structure; the feedback signal amplitude is coincidentally reduced dramatically. Moreover, due to the nonrelated irregularities in the reinforced concrete such as the presence of water and notable roughness of the structure surface, the efficacy of ultrasonic techniques have been significantly limited. These problems with conventional ultrasonic methods would disappear if the presence of concrete and other materials could be bypassed. The most promising approach lies in embedding the ultrasound device directly in the concrete–rebar structure.

Recently, embedded fiber optic devices have demonstrated their practical usages in civil engineering applications [12,13]. However, even if minimized fiber optic sensors can be implemented into concrete structures without jeopardizing its structural performance, sensing capable of effectively detecting steel rebar corrosion in concrete still cannot be achieved with existing technologies. This is because the passive sensing is not effective to detect early-stage interfacial corrosion (strain difference is too small to be detected). This paper presents a active rebar corrosion detection method using a broadband miniature fiber optic ultrasound generator [14]. This active sensing technology can be further embedded into the concrete structure for structural health monitoring (SHM). The generator's capability of rebar corrosion detection is demonstrated by identifying three prepared rebars with different levels of corrosion. This is the first step in a continuum of research to embed the fiber optic ultrasonic generator into a concrete structure for internal corrosion detection.

2. Methodology

2.1. Fiber optic ultrasonic generator

The fiber optic generator is based on the photoacoustic (PA) principle, which is an optical approach to generating ultrasound signals. The PA approach involves three steps: energy absorption, thermal expansion, and acoustic generation. The fiber optic ultrasonic generator converts pulsed laser energy exerted on the photoabsorptive thin films into thermoelastic waves [15]. The center frequency and bandwidth of the generated ultrasound is determined by the incident laser pulse [16]. The fiber optic ultrasound generator is easy to fabricate [17]. The PA generator structure is illustrated in Fig. 1. In addition, the size of each generation element, which is defined by the focal spot of a laser beam, can be easily reduced to several microns [18].

2.2. Experimental setup for corrosion reactor

The corrosion of steel in concrete structure is essentially an electrochemical process. With the presence of water, oxygen and a relevant pH value (<4), the corrosion process within the steel ordinarily coincidences with the formation of electrochemical cells with anodic and cathodic areas on the steel surface [19].

In this section, we designed an experiment to simulate and accelerate the corrosion process of a reinforced rebar. Several no. 4 steel reinforced rebars of 2 in. in length were selected as samples. An electrochemical corrosion cell in a sodium chloride solution with 15% mass concentration was utilized to facilitate the electron transfer mechanism. The schematic diagram and the photo of the corrosion reactor setup are shown in Figs. 2 and 3.

In Fig. 2, we selected our steel reinforced rebar sample as our anode and a section of copper pipe as our cathode. A potentiostat (DY 2300 Series, Digi-Ivy Inc.) with a maximum current range of ±100 mA was applied to regulate the amount of current that is impressed on the corrosion cell. An Ag/AgCl electrode with a known potential was used as a reference electrode.

2.3. Experimental setup for nondestructive corrosion detection

The schematic diagram and the experimental setup are shown in Figs. 4 and 5, respectively. All experiments were performed within a water medium. The pre-prepared rebar sample was attached to the 2-axis stepper motor stage. A 532 nm Nd:YAG nanosecond laser (Surelite I-10, Continuum) was used as the optical radiation source to couple with the FOUG. An ultrasonic pulse was generated by the FOUG and propagated through the water medium. Once the ultrasonic pulse reaches the rebar sample, the incident of pulse wave was partially reflected back as an echo signal. A hydrophone (HGL-0200, Onda) was utilized as a receiver perpendicular to the generator to collect the echo signals. Both the FOUG and hydrophone were in the same plane and placed 1 mm away from the sample. Each time the laser source emits a pulse, a signal was sent out from the laser system to trigger a data acquisition card (DAQ) (M2i.4032, Spectrum) at a sampling rate of 50 MHz. The reflected ultrasound signals were collected by the hydrophone after scanning a 1 mm by 1 mm square on the sample with a step of 250 μm. At each point, the signal was averaged for 100 times. During the experiment, the reflected ultrasound waves with large wavelength are relatively unaffected by rebar surface. In comparison, comparatively small wavelength waves tend to interact with the rebar reflection surface. That is, the degree of attenuation or scattering of reflected ultrasound signal is a function of the wavelength-to-surface roughness ratio.
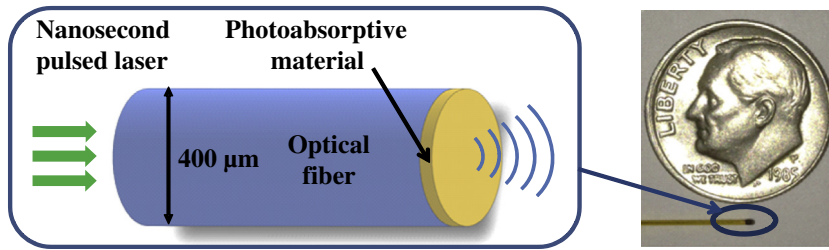
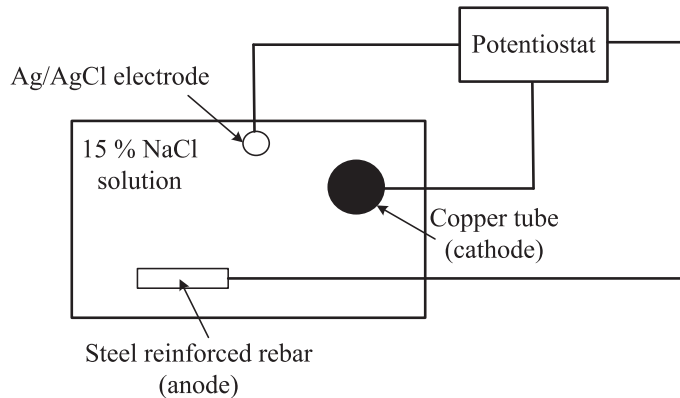**Fig. 1.** Structure of the fiber optic ultrasound generator.

Fig. 2. Schematic diagram of the corrosion reactor setup.
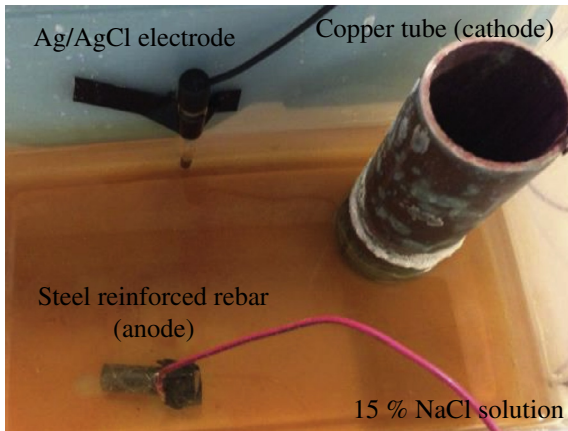

Fig. 3. Photo of the corrosion reactor setup.

3. Results and discussions

3.1. Results and discussions for corrosion reactor

Three steel rebars were used as samples in the experiment. In order to achieve the desired levels of corrosion in a timely manner, three samples were subjected to the accelerated corrosion method described above at varying time intervals. The corrosion reactor system was subjected to an average current of 99.7 mA. The corrosion rate of samples throughout the experiment was measured by calculating the mass loss and dividing it by the sample's mass prior to corrosion. After the corrosion reaction, three samples were labeled as #1, #2, and #3, which experienced a reaction time period of 24 h, 48 h, and 72 h, respectively. According to the electrochemical corrosion theory, the corrosion rate is correlated to exposure time, with rebar #1
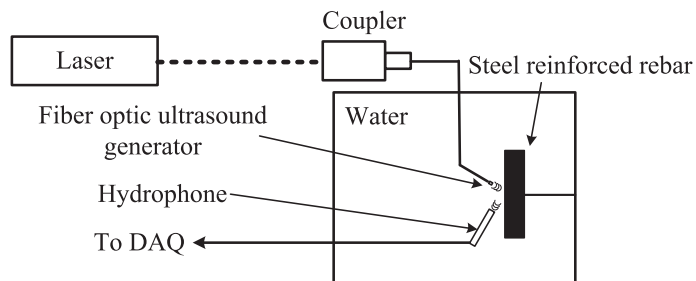

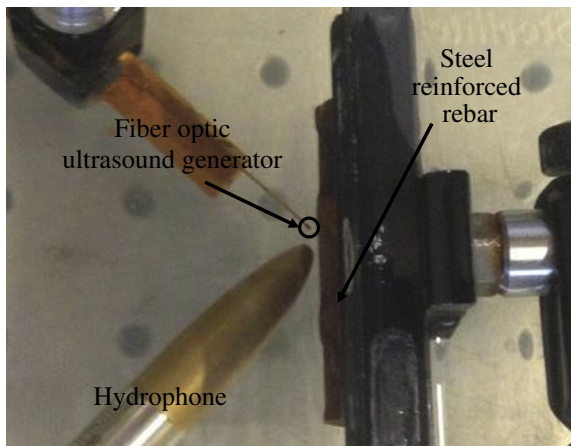**Fig. 4.** Schematic diagram of the nondestructive corrosion detection setup.

Fig. 5. The photo of the nondestructive corrosion detection setup.

Fig. 7. Corrosion rate trendline estimates from reaction time.

exhibiting the lowest corrosion rate and #3 exhibiting the highest corrosion rate in our experiment. In addition, an intact rebar has been selected as baseline and labeled as #0. The visual assessment of four samples with different corrosion rates is shown in Fig. 6. The corrosion rate of each rebar samples is presented in Table 1.

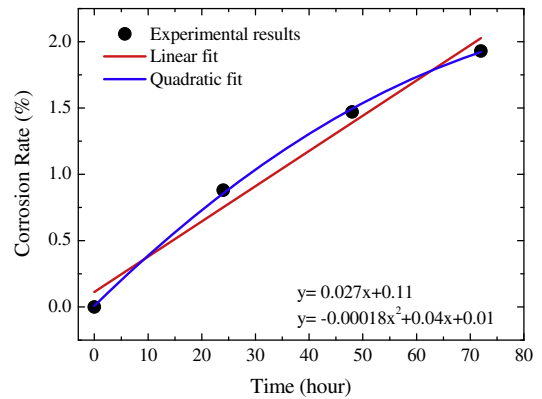Based on Refs. [20,21], the 2% mass loss would be an optimal corrosion level for our experiment; this is because

a 2% corrosion rate, typically, causes complete degradation of the rib of the rebar. As the corrosion rate further increases, the resisting force rapidly decreases. Furthermore, steel rebars with more than 12% corrosion rate indicates a brittle failure of reinforced concrete structures.

In order to investigate the relationship between the reaction time of the rebar samples and their corresponding corrosion rate, the trendline estimates from this experiment are presented in Fig. 8.

Fig. 6. The photo assessment of the samples with different corrosion rate.

Table 1
Corrosion rate of each rebar samples.

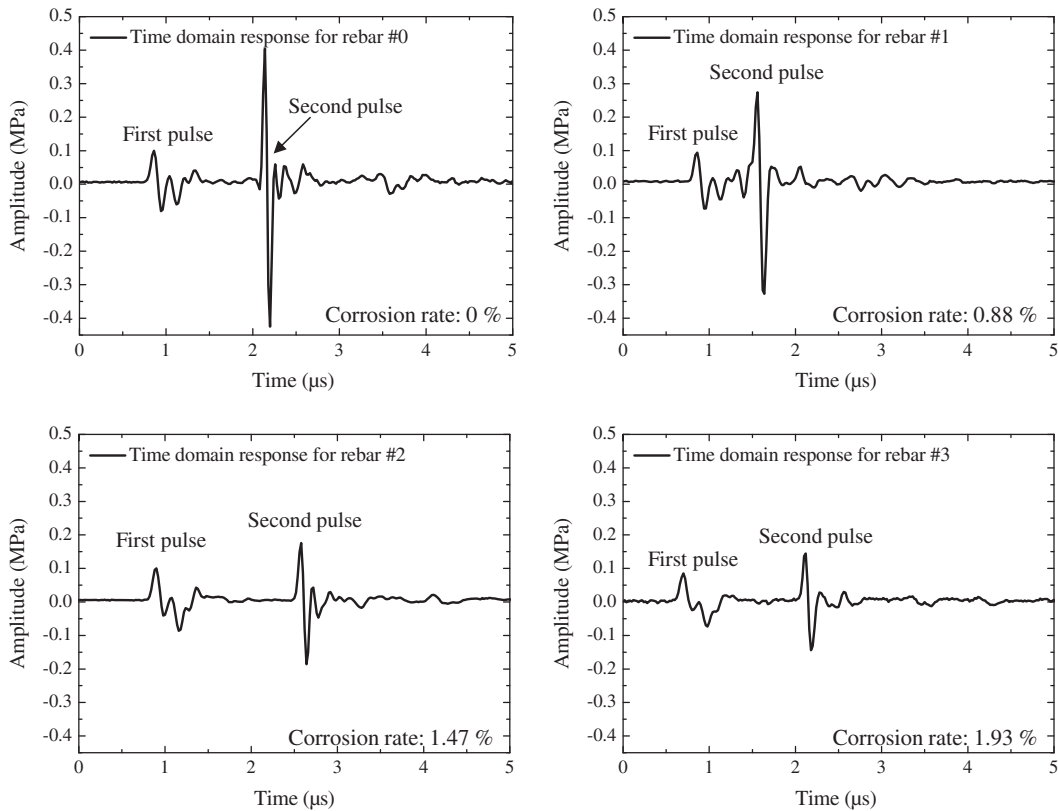| Sample label	Reaction time (h)	Mass (beginning) (g)	Mass (after reaction) (g)	Mass loss (g)	Corrosion rate (%)
Rebar #0	0	–	–	–	0
Rebar #1	24	41.95	41.58	0.37	0.37/41.95 = 0.88
Rebar #2	48	44.09	43.44	0.65	0.65/44.09 = 1.47
Rebar #3	72	48.69	47.75	0.94	0.94/48.69 = 1.93

Fig. 8. Time domain responses for rebar samples.

Using a linear fitting for the graph in Fig. 8 we have:

$$y = 0.027x + 0.11, \tag{1}$$

where x is the reaction time (in h), y is the corrosion rate (in %), R^2 is calculated as 0.97.

Using a quadratic fitting for the graph in Fig. 8 we have:

$$y = -0.00018x^2 + 0.04x + 0.01, \tag{2}$$

where x is the reaction time (in h), y is the corrosion rate (in %), the R^2 is calculated as 0.99.

From Eqs. (1) and (2), the corrosion reaction time provided a near perfect fit with the corrosion rate. From Fig. 7, the corrosion rate is primarily affected by the mass loss between predetermined time intervals measured during the experiment. This mass loss is due to the electron transfer mechanism between the cathode and the anode. The reason for using the mass loss as a corrosion rate index is that: during the corrosion reaction, the corrosion product itself becomes a passive film and slows down the corrosion rate. The instantaneous corrosion rate, therefore, does not increase with time. However, corrosion thickness loss does increase with time. This long-term trend of mass loss measurements allows us to make a better judgment in regards to the corrosion rate [22].
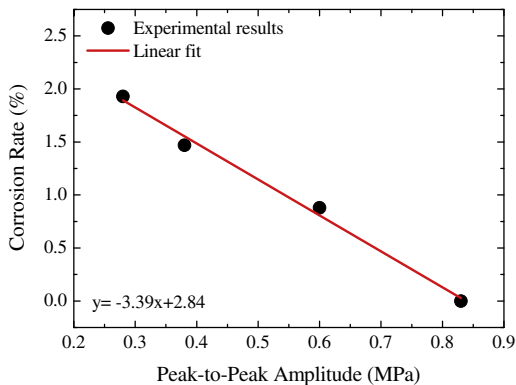

Fig. 9. Corrosion rate trendline estimates from peak-to-peak amplitude.
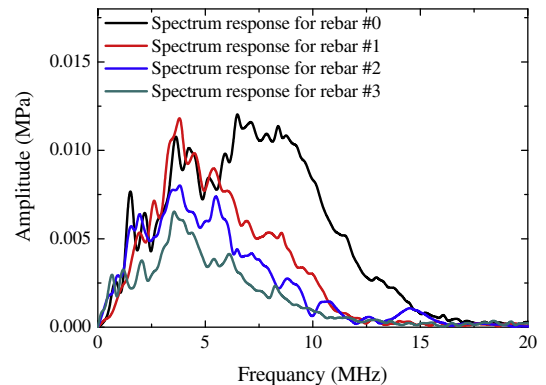

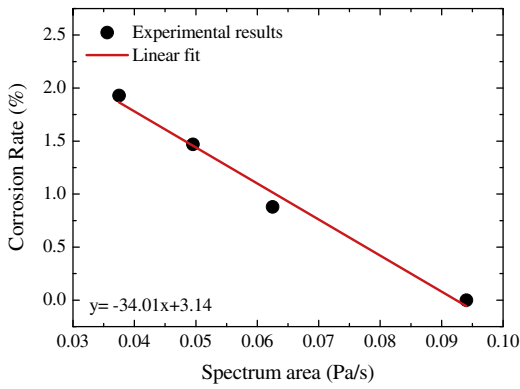**Fig. 10.** Spectrum responses for rebar samples.

Fig. 11. Corrosion rate trendline estimates from spectrum area.

3.2. Time domain responses for nondestructive corrosion detection

The time domain responses for nondestructive corrosion detection are presented in Fig. 8. For all figures, there is a set of several pulses; it can be noted that in all figures the first pulses have the similar profiles, which suggests that it is the pulse traveling directly from the PA generator to the hydrophone. The second pulses are, therefore, interpreted as the reflected ultrasound wave due to the acoustic impedance mismatch between the water and steel/rust rebar surface.

In order to investigate the relationship between the peak-to-peak amplitudes of the second pulses in the time domain responses of the rebar samples and their corresponding corrosion rate, trendline estimates are presented in Fig. 9.

Using a linear fitting for the graph in Fig. 9 we have:

$$y = -3.39x + 2.84, \tag{3}$$

where x is the peak-to-peak amplitude (in MPa), y is the corrosion rate (in %), and the R^2 is calculated as 0.99.

From Eq. (3), the peak-to-peak amplitude of the second pulses in time domain responses provided a near perfect linear fit with the actual corrosion rate data.

3.3. Spectrum responses for nondestructive corrosion detection

In order to investigate the spectral response of the rebar samples, the second pulses from Fig. 8 were examined. After performing a fast Fourier transform (FFT) of the time domain data, the spectrum responses for each rebar are shown in Fig. 10. It can be observed that the high-frequency components (6–15 MHz) of Rebar #1, Rebar #2 and Rebar #3 were attenuated due to the acoustic scattering on the corroded sample surface. Furthermore, the spectrum signals demonstrate different levels of attenuation at high frequencies, which corresponds to the samples' corrosion rates.

In order to further develop the mathematical relationship between the spectrum responses of rebar samples and their respective corrosion rates, the spectrum area is
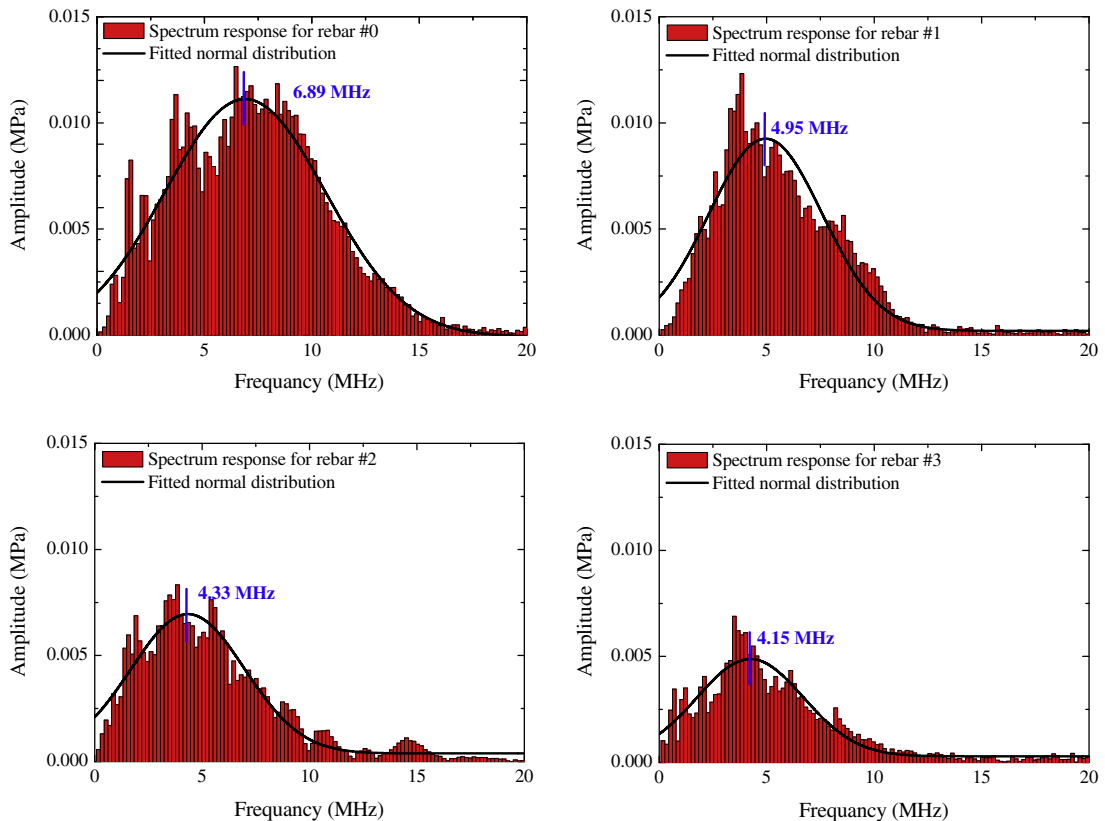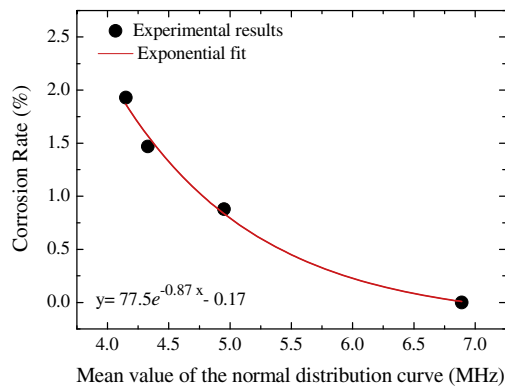

Fig. 12. Spectrum responses and the fitted normal distribution curves for rebar samples.

Fig. 13. Corrosion rate trendline estimates from mean values of the normal distribution curves.

taken into account, which represents a numerical value based on the sum of the amplitude of the weighted frequency spectrum between 0 and 20 MHz. After calculating the spectrum areas from Fig. 10, the trendline estimates are presented in Fig. 11.

Using a linear fitting for the graph in Fig. 11 we have:

$$y = -34.01x + 3.14, \tag{4}$$

where x is the spectrum area (in Pa/s), y is the corrosion rate (in %), the R^2 is calculated as 0.98. From Eq. (4), the spectrum area in spectrum responses provided a near perfect linear fit with the actual corrosion rate data.

Next, mean values of the normal distribution curves (see Fig. 12) are examined to find the relationship with corrosion rates (because the mean values represent the central frequency of the spectrum plots). With an increasing surface roughness due to the increasing corrosion rate, the central frequency of the spectrum responses was found to decrease for each rebar sample, trendline estimates are presented in Fig. 13.

Using a quadratic fitting for the graph in Fig. 13 we have:

$$y = 77.5e^{-0.87x} - 0.17, \tag{5}$$

where x is the mean value of the normal distribution curve (in MHz), y is the corrosion rate (in %), and R^2 is calculated as 0.97.

From Eq. (5) the mean value shifting provided a near perfect fit with the actual corrosion rate data. The corrosion rate can be predicted by the central frequency of the spectrum during the nondestructive corrosion detection experiment. This produced a mathematical model useful for detecting and quantifying the degree of corrosion for our application.

4. Conclusions

This paper presented the detecting and quantifying rebar corrosion by using a broadband miniature fiber optic ultrasound generator. The principle of ultrasonic corrosion detection was introduced in the first section. The experimental procedure for simulation and acceleration of the sample corrosion process by using the electrochemical process was also presented. Three steel reinforced rebar samples were prepared with different corrosion rates. The samples were characterized to demonstrate this active sensing technology is an effective method in detecting the corrosion level of steel rebar samples. The potential application is to further embed the PA device into the concrete structure for structural health monitoring.

References

[1] Z. Li, F. Li, A. Zdunek, E. Landis, S.P. Shah, Application of acoustic emission technique to detection of rebar corrosion in concrete, ACI Mater. J. 95 (1998).
[2] T. Phan, J.-L. Tailhan, P. Rossi, P. Bressolette, F. Mezghani, Numerical modeling of the rebar/concrete interface: case of the flat steel rebars, Mater. Struct. (2013) 1–15.
[3] R. Arndt, F. Jalinoos, NDE for corrosion detection in reinforced concrete structures – a benchmark approach, in: NDTCE, Nantes, France, June 30th–July 3rd, 2009.
[4] L. Bertolini, B. Elsener, P. Pedeferri, E. Redaelli, R.B. Polder, Corrosion of Steel in Concrete: Prevention, Diagnosis, Repair, Wiley.com, 2013.
[5] H.-W. Song, V. Saraswathy, Corrosion monitoring of reinforced concrete structures – a, Int. J. Electrochem. Sci. 2 (2007) 1–28.
[6] M. Montemor, A. Simoes, M. Ferreira, Chloride-induced corrosion on reinforcing steel: from the fundamentals to the monitoring techniques, Cement Concr. Compos. 25 (2003) 491–502.
[7] J.J. Beaudoin, V. Ramachandran, Handbook of Analytical Techniques in Concrete Science and Technology: Principles, Techniques, and Applications, Noyes Publications, 2001.
[8] J. Krautkrämer, H. Krautkrämer, Ultrason. Test. Mater. (1990).
[9] S. Ould Naffa, M. Goueygou, B. Piwakowski, F. Buyle-Bodin, Detection of chemical damage in concrete using ultrasound, Ultrasonics 40 (2002) 247–251.
[10] M. Schickert, Progress in ultrasonic imaging of concrete, Mater. Struct. 38 (2005) 807–815.
[11] J.R. Tucker, Ultrasonic spectroscopy for corrosion detection and multiple layer bond inspection, in: The First Joint DoD/FAA/NASA Conference on Aging Aircraft, 1997, pp. 1537–1550.
[12] X. Zou, A. Chao, Y. Tian, N. Wu, H. Zhang, T.-Y. Yu, X. Wang, An experimental study on the concrete hydration process using Fabry–Perot fiber optic temperature sensors, Measurement 45 (2012) 1077–1082.
[13] X. Zou, A. Chao, N. Wu, Y. Tian, T.-Y. Yu, X. Wang, A novel Fabry–Perot fiber optic temperature sensor for early age hydration heat study in Portland cement concrete, Smart Struct. Syst. 12 (2013) 41–54.
[14] X. Zou, N. Wu, Y. Tian, X. Wang, Broadband miniature fiber optic ultrasound generator, Opt. Express 22 (2014) 18119–18127.
[15] N. Wu, Study of a Fiber Optic Ultrasound Transducer Based on Photoacoustic Technology by Nanocomposite, University of Massachusetts Lowell, Lowell, 2012, p. 95.
[16] N. Wu, W. Wang, Y. Tian, C. Guthy, X. Wang, Theoretical analysis of a novel ultrasound generator on an optical fiber tip, Proc. SPIE 7677 (2010).
[17] X. Zou, N. Wu, Y. Tian, X. Wang, Nondestructive characterization for PDMS thin films using a miniature fiber optic photoacoustic probe, 2013, pp. 86940P–86940P.
[18] S.-W. Huang, Y. Hou, S. Ashkenazi, M. O'Donnell, High-resolution ultrasonic imaging using an etalon detector array, Appl. Phys. Lett. 93 (2008) 113501–113503.
[19] J. Gulikers, M. Raupach, Modelling of reinforcement corrosion in concrete, Mater. Corros. 57 (2006) 603–604.
[20] L. Chung, S.-H. Cho, J.-H. Jay Kim, S.-T. Yi, Correction factor suggestion for ACI development length provisions based on flexural testing of RC slabs with various levels of corroded reinforcing bars, Eng. Struct. 26 (2004) 1013–1026.
[21] L. Amleh, S. Mirza, Corrosion influence on bond between steel and concrete, ACI Struct. J. 96 (1999).
[22] C. Jaquez, Analysis of Accelerated Corrosion Experiment on Reinforced Concrete Slabs Using Half-Cell Potential Measurements, University of Massachusetts Lowell, Lowell, 2013, p. 214.